Journal of Physics and Chemistry of Solids 119 (2018) 220–227

Contents lists available at ScienceDirect

Journal of Physics and Chemistry of Solids

journal homepage: www.elsevier.com/locate/jpcs

Electronic, bonding, linear, and nonlinear optical properties of $Na_2MGe_2Q_6$ (M = Cd, Zn, Hg; Q = S, Se), $Na_2ZnSi_2S_6$, and $Na_2ZnSn_2S_6$ two metal-mixed chalcogenide compounds: Insights from an *ab initio* study

R. Mahiaoui[c], T. Ouahrani[b,c,*], A. Chikhaoui[a], A. Morales-García[d], A.H. Reshak[e]

[a] *Département de physique, Université de Tlemcen 13000, Tlemcen Algeria*
[b] *École Préparatoire en Sciences et Techniques, BP 165 R.P., 13000 Tlemcen Algeria*
[c] *Laboratoire de Physique Théorique, Université de Tlemcen 13000, Tlemcen Algeria*
[d] *Departament de Ciencia de Materials i Química Física & Institut de Química Teórica i Computacional (IQTCUB), Universitat de Barcelona, c/ Martí Franqués 1, 08028 Barcelona, Spain*
[e] *New Technologies - Research Centre, University of West Bohemia, Univerzitni 8, 306 14 Pilsen, Czech Republic*

ARTICLE INFO

Keywords:
ab initio calculation
Band structure
Bonding analysis
Second harmonic generation

ABSTRACT

In this study, in order to understand the origins of the bonding, electronic, and optical properties of $Na_2MGe_2Q_6$ (M = Cd, Zn, Hg; Q = S, Se), $Na_2ZnSi_2S_6$, and $Na_2ZnSn_2S_6$ compounds, we conducted first principles calculations within the density functional theory framework. We analyzed the sensitivity of replacing cations and anions with different electronegativity, which were rationalized in terms of the electronic structure and the contributions of different orbitals. Our calculations yielded lattice parameters, band gap, dipole moments, and second harmonic components that generally agreed well with the available experimental data. In addition, the electron localization function and atom-in-molecule topological formalisms were used to obtain further insights into the bonding properties. The calculations demonstrated the good concordance between the nature of the analyzed electronic domains and the response to second harmonic generation for the compounds studied. Moreover, the optical properties of these materials were found to be highly sensitive to the combined effects of the [Si/Ge/SnQ_4] and [MQ_4] units.

1. Introduction

Progress in nonlinear optical (NLO) research has led to the development of many important technological applications, which can be implemented when suitable materials are available. Since the discovery of excellent materials with few disadvantages, such as β-BaB_2O_4, LiB_3O_5, and $KBe_2BO_3F_2$ [1–4], an abounding new compounds [1–4], many new compounds have been synthesized with attractive NLO properties, including large NLO responses and large band gaps (possibly high laser damage thresholds). Recently, experimental studies of quaternary sulfide materials based on X-ray analysis [5–7] have identified novel compounds with a large second-harmonic generation (SHG) response, such as two metal mixed chalcogenide $Na_2ZnGe_2S_6$ [6]. According to Li et *al.*, the interesting properties that make this material useful are due to the cooperative arrangement of microscopic NLO building units, such as second-order Jahn–Teller distorted polyhedral units, and the attractive and repulsive interactions among anions/cations [8–10]. In addition, due to its wide band gap, this compound can achieve a balance between two important properties comprising a large SHG response and high laser damage threshold. These previous studies are important for the development of the NLO field, but the electronic and optical properties of this type of compound have not been investigated, and the bonding calculations have not been reported.

The possible applications of the topological measure of electron density have expanded considerably due to advances in computer resources. Recently, this analysis has been closely linked with the rigorous systematization of the elusive concept of a chemical bond and evaluations of the distributed moments in molecules and crystalline systems [11]. As an important measured/predicted descriptor, dipolar polarization is essential for understanding the origins of permanent and induced dipole moments as well as dielectric polarization in materials. Therefore, in this study, we investigated the effects of the polyhedral units in $Na_2ZnGe_2S_6$ on the SHG properties, where we considered a set of crystalline compounds with stoichiometry $Na_2MM'_2Q_6$ (M = divalent cations and M' = group 14 cations), i.e., $Na_2ZnGe_2S_6$, $Na_2ZnGe_2Se_6$, $Na_2CdGe_2S_6$, $Na_2CdGe_2Se_6$, $Na_2HgGe_2S_6$, and $Na_2HgGe_2Se_6$. These

* Corresponding author. École Préparatoire en Sciences et Techniques, BP 165 R.P., 13000 Tlemcen Algeria.
E-mail address: tarik.ouahrani@gmail.com (T. Ouahrani).

https://doi.org/10.1016/j.jpcs.2018.04.003
Received 19 December 2017; Received in revised form 25 March 2018; Accepted 7 April 2018
Available online 12 April 2018
0022-3697/

compounds were selected in order to understand the roles of the constituent cations and anions in the [GeQ_4] and [MQ_4] units, with (Q) as the anion. We calculated the linear and NLO properties based on the methods of Aspnes [12], Sipe and Gharamani [13], and Aversa and Sipe [14]. In addition, we performed accurate analyses of the structural, dynamical, and electronic properties of these compounds.

In the following, we present the basic computational methods used in this study, the calculated electronic structures, and the bonding properties based on topological analysis of the electron density and optical response. In the final section, we give a summary of the results and the main conclusions.

2. Computational modeling

The main aim of this study was to investigate the optical responses and their relationships with bonding properties. Thus, we determined the momentum matrix elements and band structures, as well as investigating the permitted inter-band and intra-band transitions that obey the selection rules [15]. Thus, we employed the accurate full all-electron potential linearized augmented planewave (FP-LAPW) method based on density functional theory (DFT) as implemented in the ELK code [16]. We used the modified Becke–Johnson exchange potential (mBJ) [17] for the exchange correlation potential. The mBJ exchange potential was accessed via an interface to the LIBXC library [18]. A satisfactory degree of convergence was achieved by considering a number of FP-LAPW basis functions up to $R_{MT} \times K_{max}$ equal to 8 (where R_{MT} is the minimum radius of the muffin tin spheres and K_{max} is the magnitude of the largest $\boldsymbol{k}$ vector in the plane wave expansion). To preserve the same degree of convergence for the *a*, *b*, and *c* lattice parameters, we kept the values of the sphere radii and K_{max} constant over all the lattice spacing range considered. However, the Fourier expanded charge density was truncated at $G_{max} = 12(\text{Ry})1/2$.

As a general guideline for local measures (electron localization function (ELF) [19], atoms-in-molecule (AIM) theory [20], and dipolar polarization), we used the Vienna *ab initio* simulation package (VASP) [21]. We utilized the projector augmented wave all-electron description of the electron–ion core interaction [21]. Total energy minimization was achieved by calculating the Hellmann–Feynman forces and the stress tensor. The optimized lattice parameters and the relaxation of the atomic positions calculated using the ELK code were reoptimized with the conjugate gradient method within VASP. Atomic relaxation was stopped when the forces acting on the atoms were less than 0.01 eV/Å. Brillouin zone integrals were approximated using the Monkhorst and Pack scheme [22], and the energies were converged with respect to the **k**-point density with a space of 0.03$Å^{-1}$. In addition, a plane-wave cutoff energy of 900 eV was required to ensure convergence. In addition to the linear response, we investigated the nonlinear response of the second order susceptibilities as well as their inter- and intra-band contributions [14], which we studied with the independent particle picture [15] implemented in ELK code.

Analyzing the bonding interactions based only on the charge density distribution may lead to the incorrect identification of the nature of chemical bonding. Thus, in order to analyze the ionic/covalent contributions to chemical bonding, we performed Bader [20] analysis based on the AIM theory. In this approach, each atom in a crystal is surrounded by an effective surface that runs through a minima region of the charge density, and the total charge of an atom (the so-called Bader charge, $Q(\Omega)$) is determined by integrating this region. Moreover, in order to measure the paired electrons, we employed the ELF designed by Becke and Edgecombe [19] according to the intuitive analysis method proposed by Savin et *al.* [23] in the DFT framework, where the ELF can be understood as a local measure of the excess local kinetic energy from electrons due to the Pauli principle. The ELF topology provides a partition into localized electronic domains known as basins. These basins are then used for rationalizing the bonding schemes in molecules and solids. The synaptic order of a valence ELF basin is the number of core basins with which they share a common boundary (zero-flux surface). Each valence basin is then represented with a chemical meaning according to the Lewis theory: a monosynaptic basin labeled V(A) in the lone-pair region of A atom or a disynaptic basin labeled V (A, B) for two-center A-B bonds. Overall, the spatial locations of basins closely match with the valence shell electron pair repulsion (VSEPR) domains [24]. The topological procedures used for AIM and ELF analyses were taken from the VASP package, and they were analyzed using the TOPCHEM code [25]. The magnitude of the dipolar electrostatic moment (noted $|\mu|$) [26–28] was calculated based on the ELF basins [11] as follows:

$$\mu_x(\Omega) = \int_{\Omega} (x - X_c)\rho(\mathbf{r})d\mathbf{r}^3 \quad (1)$$

$$\mu_y(\Omega) = \int_{\Omega} (y - Y_c)\rho(\mathbf{r})d\mathbf{r}^3 \quad (2)$$

$$\mu_z(\Omega) = \int_{\Omega} (z - Z_c)\rho(\mathbf{r})d\mathbf{r}^3 \quad (3)$$

where X_c, Y_c, Z_c are the Cartesian coordinates of the nuclear centers. $|\mu|$ was then calculated as the square root of the sum of the squared components. Due to the invariance of $|\mu|$ with respect to the orientation of the system's axis, it was then feasible to compare the polarization lone pairs in different chemical environments [29].

3. Results and discussion

3.1. Ground state properties

According to experimental evidence [6], the structure of the selected compounds ($Na_2MGe_2Q_6$) (Fig. 1(a)) could be described as particular three-dimensional tunnel cages. The first comprises infinite $\infty[GeQ_3]_n$ chains and isolated [ZnQ_4] tetrahedra. The second is built from edge-shared Na (1)Q_5 polyhedra and Na (2)Q_6 octahedra (Na (1) and Na (2) correspond to the two different Wyckoff positions of the sodium atom), whereas the germanium cations are aligne as fourfold

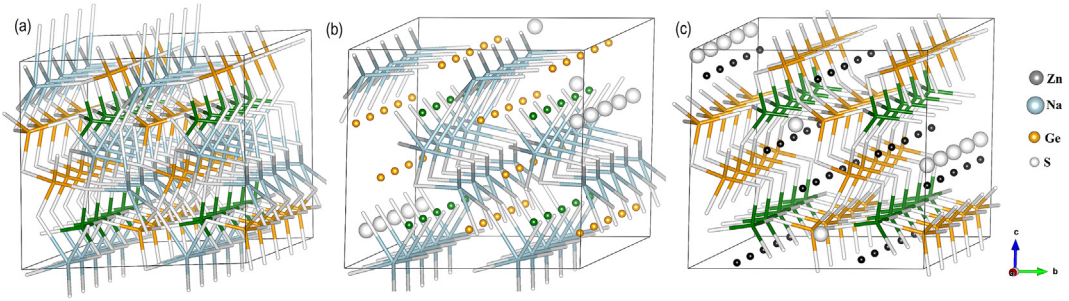

Fig. 1. The 4 × 1 × 1 structure of the $Na_2ZnGe_2S_6$ compound. It is possible to distinguish: (a) the three-dimensional tunnel structure formed by $\infty[GeQ_3]_n$ chains, (b) two types of Na polyhedra, and (c) distorted [GeS_4] tetrahedra connected with [ZnS_4] tetrahedra by sharing the corner of S atoms.

Table 1
Calculated lattice parameters *a*, *b*, and *c* (in Angstroms), *β* angle, and elastic constants ($\mathbb{C}_{ij}$ in GPa) for the compounds investigated in the monoclinic **Cc** phase.

a	*b*	*c*	*β*	C_{11}	C_{12}	C_{13}	C_{15}	C_{22}	C_{23}	C_{25}	C_{33}	C_{35}	C_{44}	C_{46}	C_{55}	C_{66}
$Na_2ZnGe_2S_6$																
7.41	12.59	11.80	102.69	28.24	24.12	16.07	5.07	42.56	17.32	8.19	40.89	2.93	12.90	1.85	−0.52	11.01
7.28[a]	12.35[a]	11.45[a]	100.63[a]													
$Na_2ZnGe_2Se_6$																
7.74	13.22	12.40	102.46	21.28	19.42	12.96	3.84	34.43	13.91	5.29	32.18	2.68	9.75	1.5	0.33	8.46
$Na_2CdGe_2S_6$																
7.42	12.78	11.76	98.74	28.47	23.42	17.34	2.62	42.54	22.04	2.7	40.35	−0.1	10.53	2.45	5.14	9.47
7.31[b]	12.67[b]	11.53[b]	98.87[b]													
$Na_2CdGe_2Se_6$																
7.75	13.44	12.35	98.86	20.93	17.52	12.93	2.9	31.64	16.04	3.09	31.51	0.78	8.21	1.84	3.07	7.82
7.59[b]	13.18[b]	12.07[b]														
$Na_2HgGe_2S_6$																
7.42	12.85	11.78	98.98	26.84	22.89	17.14	2.34	40.00	21.17	2.82	36.09	−0.1	9.13	2.22	3.72	8.67
$Na_2HgGe_2Se_6$																
7.74	13.55	12.43	100.15	19.19	17.32	12.62	2.69	29.24	15.00	3.76	27.98	1.22	6.96	1.7	1.39	6.68
$Na_2ZnSi_2S_6$																
7.38	12.29	11.48	102.33	25.64	22.35	11.56	2.22	23.54	14.11	2.86	24.33	−0.1	6.12	1.12	−0.13	6.13
$Na_2ZnSn_2S_6$																
7.44	13.21	12.48	105.56	33.22	30.12	17.11	5.50	43.86	17.95	8.64	42.11	3.74	13.24	2.22	−0.47	11.56

[a] Quoted from Ref. [6].
[b] Quoted from Ref. [7].

polyhedra within the anions (Q) (Fig. 1(c)). The Zn cations are also connected with four Q anions, which act as the linkers among the wave-like infinite $\infty[GeQ_3]_n$ chains, and they comprise a three-dimensional tunnel structure. The Na cations point in the tunnels and they have two different coordination environments, which include a highly distorted Na (1)Q_5 unit. It should also be noted that the Na (1)Q_4 and Na (2)Q_6 units in the same tunnel are connected with each other in an alternate manner by sharing corners to form [Na (1)–cation–Na (2)]$_n$ spiral chains along the **a**-axis (Fig. 1(b)). These alternations in different tunnels interlink with each other via anions to make another three-dimensional tunnel framework. This environment means that these structures belong to polar non-centrosymmetric space group **Cc** (No. 9) in symmetry class (m). The interplay between [ZnQ_4] and [GeQ_4] tetrahedra in this non-centrosymmetric arrangement increases the NLO properties of the system. Full geometrical optimization was needed because of this rather complicated architecture, and thus we conducted extensive numerical optimization and relaxation in order to ensure the stability of the zero pressure equilibrium structures. The predicted values are presented in Table 1. The juxtaposition with the available structural properties of $Na_2ZnGe_2S_6$, $Na_2CdGe_2S_6$, and $Na_2CdGe_2Se_6$ indicates that our theoretical calculations are close to the previously reported experimental results [6,7].

In order to understand the mechanical stability of these compounds, we computed the elastic constants from the linear response of density functional perturbation theory (DFPT) calculations. The elastic constants of a material describe its response to an applied stress or the stress required to maintain a given deformation. Both the stress and strain have three tensile constants and three shear constants from a 6 × 6 symmetric matrix, with 27 different components, where 21 are independent. However, any symmetry present in the structure may reduce the number of these components. The well-known Born stability [30] criteria for a monoclinic system are as follows [31,32].

$$C_{11} > 0,\ C_{22} > 0,\ C_{33} > 0,\ C_{44} > 0,\ C_{55} > 0,\ C_{66} > 0,$$

$$(C_{11} + C_{22} + C_{33} + 2C_{12} + 2C_{13} + 2C_{32}) > 0,$$

$$(C_{33}C_{55} - C_{35}^2) > 0,\ (C_{44}C_{66} - C_{46}^2) > 0,$$

$$(C_{22} + C_{33} - 2C_{23}) > 0,$$

$$[C_{22}(C_{33}C_{55} - C_{35}^2 + 2C_{23}C_{25}C_{35} - C_{23}^2C_{55} - C_{25}^2C_{33})] > 0,$$

$$\{2[C_{15}C_{25}(C_{33}C_{12} - C_{13}C_{23}) + C_{15}C_{35}(C_{22}C_{13} - C_{12}C_{23}) +$$

$$C_{25}C_{35}(C_{11}C_{23} - C_{12}C_{13})]$$

$$- [C_{15}^2(C_{22}C_{33} - C_{23}^2) + C_{25}^2(C_{11}C_{33} - C_{13}^2) +$$

$$C_{35}^2(C_{11}C_{22} - C_{12}^2)] + C_{55}(C_{11}C_{22}C_{33} - C_{11}C_{23}^2 - C_{22}C_{13}^2 -$$

$$C_{33}C_{12}^2 + 2C_{12}C_{13}C_{23}) > 0\} \quad (4)$$

All the conditions required for mechanical stability given in Equation (4) were simultaneously satisfied, which clearly indicates that the predicted structures are mechanically stable phases. According to the conditions given above, both selenium and sulfur based compounds match the equilibrium stability for the monoclinic **Cc** structure. However, should be noted that other structures [5,33] could exist with other symmetrical groups. In fact, $Na_2CdGe_2Se_6$ and $Na_2ZnGe_2Se_6$ were previously synthesized in a tetragonal (**I4/mcm**) system [5] and $Na_2ZnSn_2S_6$ in an Fdd2 system [7]. This is due to the different connection types for the building blocks (more flexible corner-sharing type in **Cc** but tight edge-sharing type in **I4/mcm**, or with a different arrangement in **Fdd2**). However, this issue is outside the scope of the present study.

3.2. Band structure and orbital contributions

To obtain a quantitative understanding of the electronic properties of the tilted structures, we calculated their band structures based on the mBJ potential. All of the structures had a direct band-gap (E_g) at the (Γ−Γ) point and their values are shown in Table 2. The calculated

Table 2
Band gap energy (E_g) calculated at the mBJ level where the values are compared with the variable values given in a previous study [6].

	E_g (eV)
$Na_2ZnGe_2S_6$	3.21, 3.25[a]
$Na_2ZnGe_2Se_6$	2.22
$Na_2CdGe_2S_6$	3.31, 2.6[b]
$Na_2CdGe_2Se_6$	2.25, 1.94[b]
$Na_2HgGe_2S_6$	3.04
$Na_2HgGe_2Se_6$	2.08
$Na_2ZnSi_2S_6$	4.31

[a] Quoted from Ref. [6].
[b] CASTEP-VASP from Ref. [7].

band-gap value for the $Na_2ZnGe_2S_6$ compound was in good agreement with the experimental value. However, the values for $Na_2CdGe_2S_6$, and $Na_2CdGe_2Se_6$ appeared to be higher than the theoretical values obtained with the traditional GGA exchange correlation approach. The relatively wide band gap determined for the materials based on the sulfur anion is a prerequisite for infrared NLO applications [34]. In addition, to understand the orbital contribution of each band, we generated the band structure plots with the orbital-projected components, where the colored circles, triangles, and squares represent the group-*s* and *p*, and *d* states, respectively, and the symbol size is proportional to the orbital weight in Fig. 2(a). Furthermore, we also plotted the orbital isosurface for the highest and lowest occupied molecular orbitals (HOMO and LUMO, respectively) (Fig. 2(b–g)). We found that all of the tilted compounds had the **Cc** structure for the same ground and band-orbital reorganization along the high-symmetry path curve. Thus, in the orbital analysis, we represented the plot of $Na_2ZnGe_2S_6$ as a prototype (Fig. 2).

Fig. 2(a) shows clearly that the conduction band originates from the Ge-*p* orbitals. However, the HOMO is derived primarily from the non-bonding Ge-4s orbitals and the LUMO is primarily derived from the S-3*p* orbitals. Thus, the HOMO-LUMO energy gap can be used as a measure of the energy of the charge transfer from the sulfur orbitals to the germanium orbitals. These orbitals are mostly involved in the allowable transitions because they build up the polarizability pattern. Our analysis of the orbital contribution of each band for all the compounds showed that the valence band can be divided into three sub-bands, i.e., the lowermost, middle, and uppermost bands. The lowermost band is mostly due to the hybridization of the Ge-*s*, Ge-*p*, and S-*s* states (not shown in Fig. 2(a)). The middle band is predominately due to the M-*d* (M = Zn, Cd and Hg) and Ge-*s* states. The uppermost valence band at the Fermi level is predominantly due to Ge-*p*, with a considerable contribution from Q-*p* (Q = S and Se) states. The main result is the difference in the band gap value when the sequence anion moves from S to Se (Table 2 and Fig. 3(a–c)). This difference is due to the Ge-*d* orbital interacting strongly with the Q-*p* orbitals and to the differences in hybridization related directly to the atomic chalcogenide radius (the tables from the Supplementary materials in (6) show clearly that S has a valence of 3*p* and Se 4*p* orbital). The integration of the orbital population illustrates this difference (see the tables in the Supplementary materials in (6)). The interaction with the orbital mainly involves Ge-4*p*-4d with $3p_{zx}$, $4p_{zx}$, and $5p_{xy}$ for the S and Se anions. This strong hybridization between the orbitals decreases the band gap value. Interestingly, among all the changes in the band gap value, the replacement of the divalent cation M from Zn with Hg produces only a very slight difference in the value of E_g. In the analysis, we also used our new predictions as inputs. We replaced the Ge cation using metals with equal electronegativity, i.e., Sn and Si, while keeping the anion S fixed (Fig. 3(e–f)). In contrast to replacing the divalent atom, the cation from column XIV affects the strongly orbital contribution in both the conduction and middle valence sub-bands. Hence, the changes in the electronic properties are attributable to the hybridization between the M-*d* and M′-*s* states, which shift this sub-band over the Fermi level, thereby favoring the interaction between the HOMO and LUMO orbitals.

3.3. Bonding analysis

It is well known that in DFT calculations, analyzing the electron density in real space approaches is essential for determining the ground-state properties of a compound. This analysis is required because the valence electrons are involved in the band gap as well as the optical quantities, such as the dipole moments and related derivatives [35]. Thus, to determine the relationships between the band gap, linear and NLO properties, and the inherent organization of electrons in the tilted compounds, we used state-of-the-art quantum interpretative techniques combined with ELF/AIM computations, thereby capturing all the ranges of the chemical quantities in the structures of the compounds. The electron localized domains induced by the ELF measure were determined for the sulfur-based compounds with the M′ cation as Si, Ge, and Sn. The ELF bonding isosurfaces of these compounds are shown in Fig. 4. These plots indicate that the domain of electronic localization is formed from three types of disjoint basins, which are distributed polyhedrically around the Q anion. The two disynaptic basins following the bond axis form the Zn–Q and Na–Q bonds, and another with a smaller shape is present in the middle of the Ge-Q bond. Ge-Q has a polarized covalent character, whereas the other basins are polarized and also deformed. Furthermore, due to the non-spherical behavior of the Q anionic basin, the ELF topology shows that some structural changes occur, which confirms the mainly ionic character of both the Zn–Q and Na–Q bonds [36].

The isosurfaces of $Na_2ZnSi_2S_6$, $Na_2ZnGe_2S_6$, and $Na_2ZnSn_2S_6$ are depicted in Fig. 4, where the M′–S bond (basin) is highlighted. Clearly, the compound based on the Sn cation has a different orientation for its polyhedra. Thus, in order to achieve an accurate description of the bonding characters of the $M'Q_4$, NaQ_5, and MQ_4 polyhedra, we integrated the population over all the ELF basins. As expected, we found that the polarization in the Na valence basin is weak and most of its electrons are transferred to the anion one, which makes the disynaptic valence basin V(Na,Q) larger with an important population (the average values for the three cases of Q, $\overline{N}$~5.74 electrons) (Fig. 4). The figure shows that the topological domain of Q atom is strongly polarized along the Q–M′ axis and it broadly encloses the ELF domains

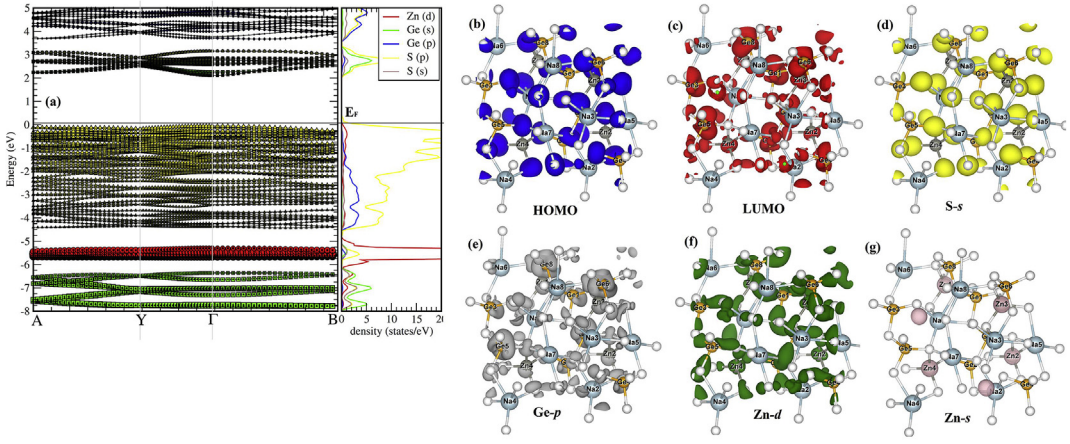

Fig. 2. Plot (a) shows the band structure of the $Na_2ZnGe_2S_6$ in the Generalized Gradient Approximation (GGA) exchange correlation level, where the bands are colored to distinguish the orbital contribution of each atom. Plots (b–g) represent the isosurfaces of the constituent orbitals in (a).

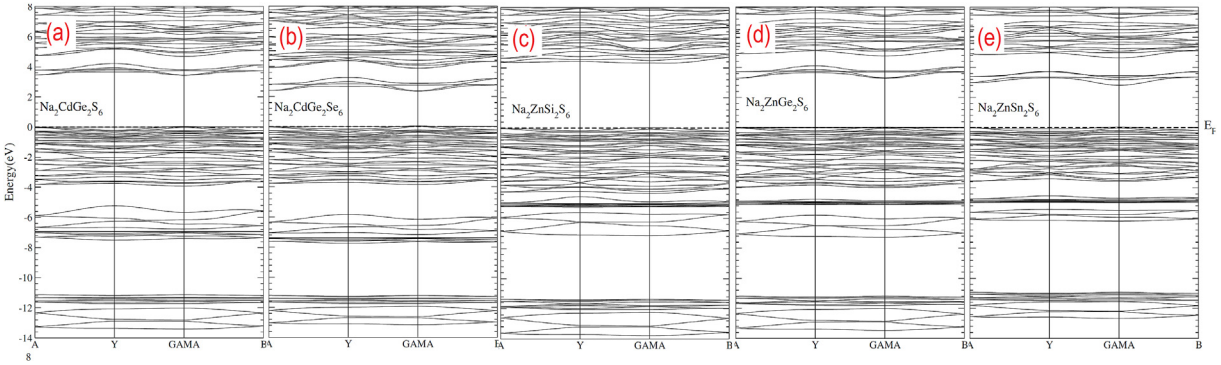

Fig. 3. Band structure plots at the mBJ level for: (a) $Na_2ZnGe_2S_6$, (b) $Na_2ZnGe_2Se_6$, (c) $Na_2ZnSi_2S_6$, (d) $Na_2ZnGe_2S_6$, and (e) $Na_2ZnSn_2S_6$ compounds.

around the Q anion, but without overlapping with the nearby atoms (M and Na). Thus, the M–Q domain has 2.24 electrons whereas the M′–Q domain has 2 electrons, which typically corresponds to a single covalent bond. The bond polarity indexes of the three disynaptic basins V (S–M′) are P_{Si-S} = 0.88, P_{Ge-S} = 0.89, and P_{Sn-S} = 0.96, which reflect the increases in the polarization between the atoms forming the polarized covalent S–M′ bonds. Due to the differences in electronegativity between the atoms forming the bonds and the nature of the chemical environment, it is essential to integrate the dipole moment. Thus, in order to compare our results with those obtained in a previous study [6], we calculated the magnitude of the dipolar electrostatic moment (μ) for each core and valence basin. Table 3 shows that our values agree well with those obtained by Li et *al.* [6]. However, according to Table 3, we can conclude that the dipole (μ) is affected more by replacing an anion with another anion than by replacing a cation M′ with another cation. This behavior was also established by comparing the value of μ for $Na_2ZnGe_2S_6$ [6] and $Na_2ZnSn_2S_6$ [7] in previous studies with different synthesized structures. Metals such as Ge, Si, and Sn, tend to form distorted MQ_4 tetrahedra [37–39], and they help to construct a polar structure. However, it should be noted that both the tendency of an element to gain or lose electrons (the outer-core states) and of the neighbors to influence an element are important for the construction of the dipolar polarization moment. In fact, the M′ cation can be replaced by another with the same electronegativity but the nature of the bond is changed, probably because of the nature of the interactions between the polyhedra. Therefore, μ is more pronounced when the cation is bonded to a more electronegative anion. However, all of the results based on the dipole moments and ELF topology demonstrate that the large NLO response is mainly attributable to the cooperative effects of the [M'Q_4] and [MQ_4] units.

Table 3
Local dipole moment (μ in Debye) calculations for: $Na_2ZnGe_2S_6$, $Na_2ZnGe_2Se_6$, $Na_2ZnGe_2Te_6$, $Na_2ZnSi_2S_6$, and $Na_2ZnSn_2S_6$ compounds.

	μ(Na (1)S_6)	μ(Na (2)S_6)	μ(Ge (1)S_4)	μ(Ge (1)S_4)	μ(Zn (1)S_4)
$Na_2ZnGe_2S_6$	25.661[a], 23.33[b]	13.856[a], 28.28[b]	65.324[a], 67.68[b]	75.470[a], 76.36[b]	54.224[a], 51.60[b]
$Na_2ZnGe_2Se_6$	34.291[a]	22.206[a]	77.587[a]	81.127[a]	63.703[a]
	μ(Na (1)S_6)	μ(Na (2)S_6)	μ(Si(1)S_4)	μ(Si(1)S_4)	μ(Zn (1)S_4)
$Na_2ZnSi_2S_6$	17.991[a]	12.591[a]	15.705[a]	24.839[a]	11.308[a]
	μ(Na (1)S_6)	μ(Na (2)S_6)	μ(Sn(1)S_4)	μ(Sn(1)S_4)	μ(Zn (1)S_4)
$Na_2ZnSn_2S_6$	29.310[a]	14.536[a]	38.165[a]	66.582[a]	9.786[a]

[a] Calculated.
[b] Quoted from Ref. [6].

3.4. Optical properties

Next, we present the linear optical properties determined for the tilted compounds. Based on the mBJ calculations of the band structures, we employed the permitted transitions, i.e., the intra- and inter-band contributions, to construct the shape of the imaginary part of the dielectric susceptibility (Fig. 5). Due to the symmetry of the structure (point group C_s(m)), three tensor components are needed to complete the description of the optical properties: *xx*, *yy*, and *zz*. According to Fig. 5, it is clear that replacing the anion S and then Se leads to a decrease in the position of the threshold energy, thereby indicating the presence of Γ_v–Γ_c splitting and this accounts for the direct optical transitions between the highest valence band and the lowest CB. This is recognized as the fundamental absorption edge. The origin of this edge is associated with the inter-band transitions and the interchange from occupied Q-*p* states to the unoccupied Ge-4s and Zn-*p* states. Hence, due to the orbital interactions and the difference in electronegativity between the atoms forming the LUMO and HOMO states, the electron from these bands can redistribute the charge density and change the

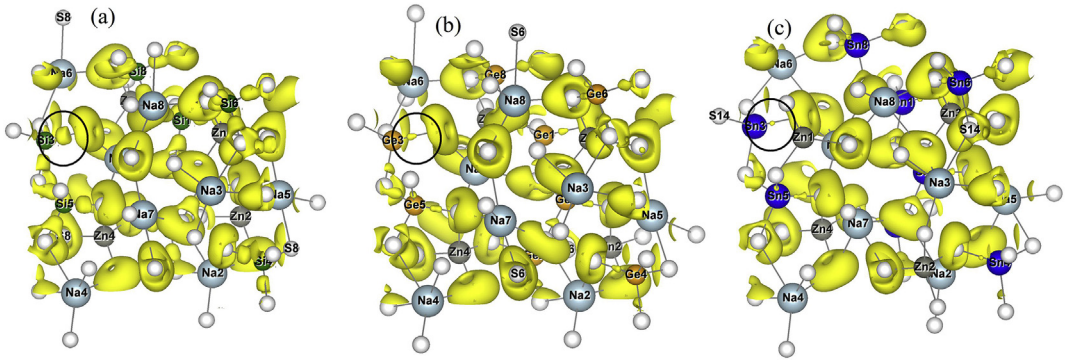

Fig. 4. ELF localization domains (ELF = 0.84) for: (a) $Na_2ZnSi_2S_6$, (b)$Na_2ZnGe_2S_6$, and (c) $Na_2ZnSn_2S_6$ compounds. The Si–S, Ge-S, and Sn–S bonds are circled to highlight the change in the basin volume.

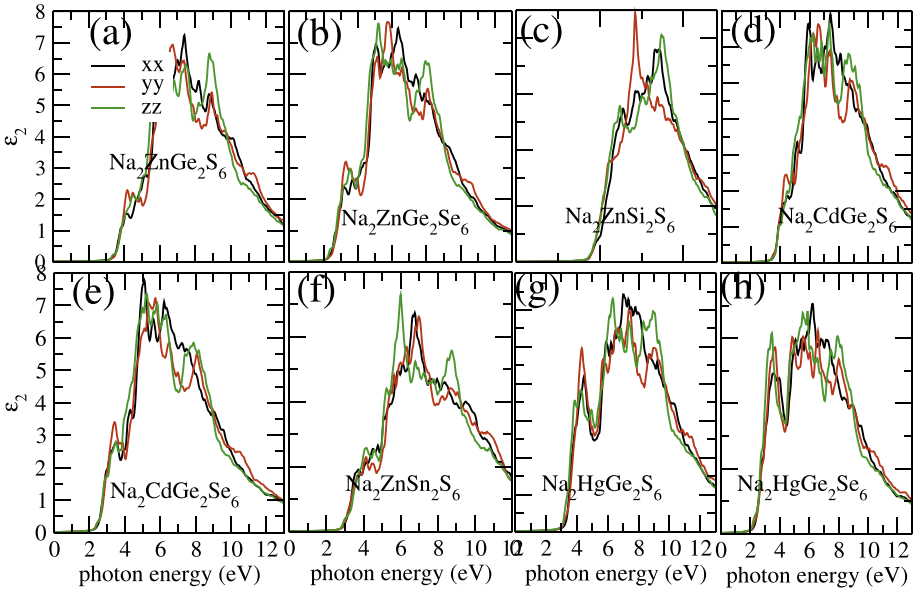

Fig. 5. Imaginary part of the dielectric function ε_2 for $Na_2MGe_2Q_6$ (M = Cd, Zn, Hg; Q = S, Se), $Na_2ZnSi_2S_6$, and $Na_2ZnSn_2S_6$ two metal-mixed chalcogenide compounds. *xx*, *yy*, and *zz* denote the ε_2^{xx}, ε_2^{yy}, and ε_2^{zz} tensor components, respectively.

dipole moment considerably. The non-centrosymmetric structure of the compounds exhibits considerable anisotropy, which is more pronounced between the absorptive parts ε_2^{yy} and ε_2^{zz}. There are also more peaks in ε_2 for compounds based on the divalent Hg cation compared with the shape of the spectra for the others. This difference is due mainly to charge transfer between electron-donating group and the electron-accepting group, which differs among divalent cations (due to the sizes of the Zn, Cd, and Hg cations).

Next, we consider the SHG responses of the crystals. First, from a theoretical perspective, the physical interpretation of the nonlinear results is very difficult because in addition tothe valence–valence and conduction–conduction transitions, both inter- and intra-band transitions can participate in the nonlinear responses. Furthermore, 2ω and ω resonances appear in the imaginary and real parts of $\chi^{(2)}$, so the second order susceptibilities ($\chi^{(2)}$) are highly sensitive to minor changes in the band dispersion. However, there is good correspondence between the nonlinear structures and those of the linear spectra as a function of both ω and 2ω [40]. The space group **Cc** allows 10 independent non-zero tensor components. However, our tilted compounds belong to the C_s class, so under the restriction of Kleinman's symmetry [41], only six SHG tensor components remain, i.e., $\chi^{(2)}_{111}$, $\chi^{(2)}_{122}$, $\chi^{(2)}_{133}$, $\chi^{(2)}_{113}$, $\chi^{(2)}_{223}$, $\chi^{(2)}_{333}$ (we use the notation: 1 = *x*, 2 = *y*, and 3 = *z*). Qualitative comparisons with the available results for the $\chi^{(2)}$ components at $\lambda = 1064$ nm are shown in Table 4. We use the notation given by [6], $d_{iL} = \chi^{(2)}/2$, where the elements are linked by the correspondence $jk \rightarrow L$. The similarity between our results and those given by [6] allowed us to confirm the good agreement between their (GGA-based) values and our (mBJ-FP-LAPW) calculations (some discrepancies were noted due to the different approaches employed). The analysis of the SHG spectra in Fig. 6(a) shows that $\chi^{(2)}_{333}$ is the dominant component of the second order susceptibility. The inset in Fig. 6(b) also shows that changing (replacing) the anion from S to Se strongly enhances the SHG response. However, replacing the cation Ge with Si or Sn also affects the magnitude of the spectra, thereby confirming the results given above. Fig. 7(a) shows the analysis of the band-to-band contributions to ω and 2ω in terms of $\chi^{(2)}_{333}$ for the $Na_2ZnGe_2Se_6$ compound. As expected, the locations of the structures in both parts of $\chi^{(2)}_{333}$ are in agreement with those in ε_2 [40]. The threshold for the two-photon 2ω parts occurs at half the energy of the threshold for the one-photon ω part. The plot exhibits the highly dispersive behavior with a notable contribution from 2ω inter/intra terms below the fundamental energy band gap (E_g). The ω resonance begins to contribute for energy values above E_g. Fig. 7 also shows the opposite symmetrical patterns determined for the ω- and 2ω-resonances at higher energies, which make the high-energy nonlinear response decrease.

4. Conclusion

In this study, we investigated the effects of replacing chalcogenide anions and metallic M/M′ cations on the electronic, bonding, and optical properties of non-centrosymmetric $Na_2MM_2Q_6$ two metal-mixed chalcogenide compounds. We used theoretical techniques including *ab initio* DFT calculations and analysis based on the topology of electron densities. Both AIM and ELF provided adequate and unambiguous descriptions of the nature of the bonding properties in the compounds. Furthermore, we showed that the framework of orbital decomposition

Table 4
SHG coefficients calculated at $\lambda = 1064$ nm for the tilted compounds. All of the d iL coefficients are shown in (pm/V) units.

	d_{11}	d_{12}	d_{13}	d_{15}	d_{24}	d_{33}
$Na_2ZnGe_2S_6$	−4.39,-4.3[a]	5.32,4.63[a]	−4.90,-5.3[a]	−4.42,-4.3[a]	4.21,4.63[a]	−3.11,-5.3[a]
$Na_2ZnGe_2Se_6$	−7.89	5.43	−12.19	−6.73	5.19	−4.09
$Na_2CdGe_2S_6$	−5.21	6.54	−5.78	−4.96	4.95	−4.57
$Na_2CdGe_2Se_6$	−6.47	5.84	−11.23	−7.13	6.21	−4.60
$Na_2HgGe_2S_6$	−6.02	6.94	−5.98	−5.16	5.19	−4.87
$Na_2HgGe_2Se_6$	−7.97	7.43	−11.53	−7.57	6.88	−4.98
$Na_2ZnSi_2Se_6$	−4.23	1.44	−4.64	−3.98	3.88	−3.5
$Na_2ZnSn_2Se_6$	−5.32	5.38	−12.85	−4.96	4.48	−4.77

[a] Quoted from Ref. [6].

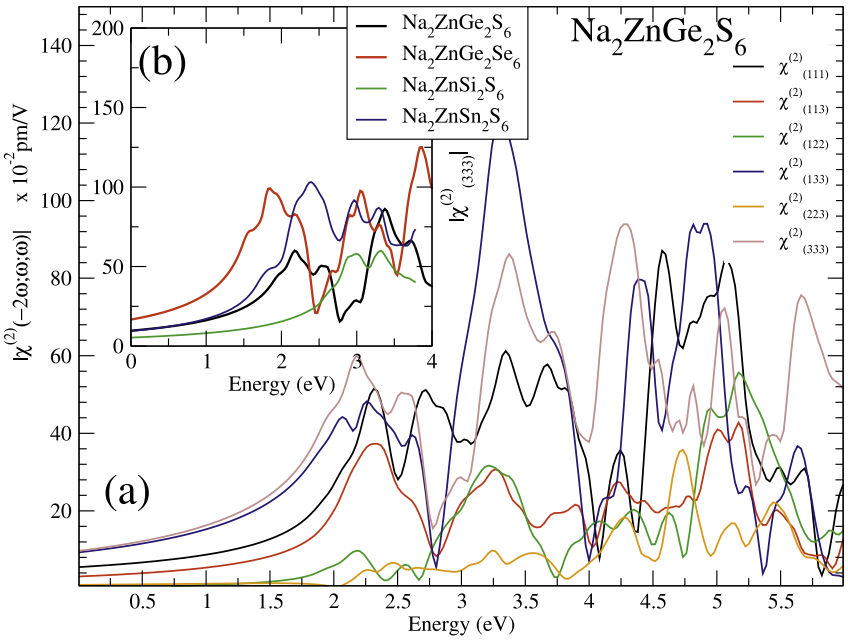

Fig. 6. (a) Absolute values of the second order susceptibility $\chi^{(2)}$ for the $Na_2ZnGe_2S_6$ compound. (b) Absolute values $|\chi^{(2)}_{333}|$ for the $Na_2ZnGe_2S_6$, $Na_2ZnGe_2Se_6$, $Na_2ZnSi_2S_6$, and $Na_2ZnSn_2S_6$ compounds.

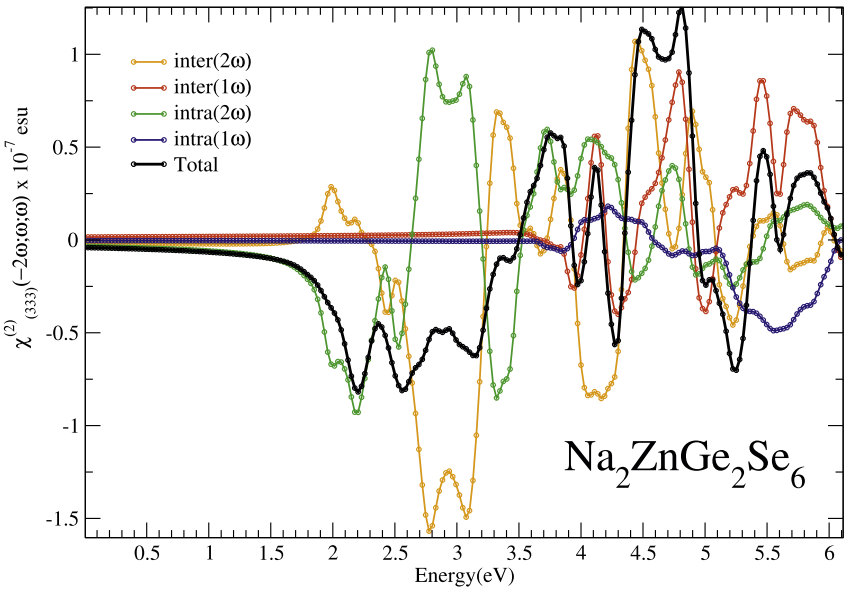

Fig. 7. Calculated total and imaginary parts of the $\chi^{(2)}_{333}$ spectrum as well as the intra- 2 ω/ω- and inter- $2\omega/\omega$ -band contributions for the $Na_2ZnGe_2Se_6$ compound. All (Im) $\chi^{(2)}$ values are multiplied by 10^{-7} in ESU units.

and microscopic viewpoint of bonding quantities are very useful tools for analyzing and explaining the changes in the orbital and band gap values after replacing cations and anions. In fact, the results suggest that the electronic properties of the tilted compounds are more strongly affected by the replacement of chalcogenide S, Se, and Te than by the divalent cations (Zn, Cd, and Hg). However, we note that replacing the cation XIV using another with the same electro-negativity could have a non-negligible effect on the electronic properties of the materials. In addition, our analysis of the electron localization domains provided insights into the bonding behavior changes after replacement (substitution). We found that the electronegativity was more pronounced when the bond was more ionic. As also shown by [6], the cooperative effects of the MQ_4 and $M'Q_4$ tetrahedral units are crucial for the dipolar polarizability in the predicted structures and they are probably due to weak interactions between polyhedra. Moreover, we studied the linear optical and NLO properties of the compounds. According to our results, the specific anionic position of the chalcogenide can enhance the anisotropy between the dielectric function components, thereby inducing a strong SHG response. Thus, we consider that our findings may motivate further experimental investigations to predict new non-centrosymmetric materials with excellent NLO properties.

Acknowledgements

We thank the MALTA Consolider Team and Departamento de Química Física y Analítica, Universidad de Oviedo (Spain), especially Professor J.M. Recio, for giving us access to the computational facilities. A. H. R. would like to acknowledge the CENTEM project, reg. no.

CZ.1.05/2.1.00/03.0088, cofunded by the ERDF as part of the Ministry of Education, Youth, and Sports OP RDI programme, and in the follow-up sustainability stage, financial support through CENTEM PLUS (LO1402) from the Ministry of Education, Youth, and Sports under National Sustainability Programme I as well as MetaCentrum (LM2010005) and CERIT-SC (CZ.1.05/3.2.00/08.0144) infrastructure.

Appendix A. Supplementary data

Supplementary data related to this article can be found at http://dx.doi.org/10.1016/j.jpcs.2018.04.003.

References

[1] V.G. Dmitriev, G.G. Gurzadyan, D.N. Nikogosyan, D.N. Nikogosyan, Handbook of Nonlinear Optical Crystals, Springer, 2013, p. 417.
[2] G.D. Boyd, Robert C. Miller, K. Nassau, W.L. Bond, A. Savage, $LiNbO_3$: an Efficient phase matchable nonlinear optical material, Appl. Phys. Lett. 5 (1964) 234.
[3] C. Chen, Y. Wu, A. Jiang, B. Wu, G. You, R. Li, S. Lin, New nonlinear-optical crystal: LiB_3O_5, J. J. Opt. Soc. Am. B 6 (1989) 616.
[4] Y.N. Xia, C.T. Chen, D.Y. Tang, B.C. Wu, New nonlinear-optical crystals for UV and VUV harmonic-generation, Adv. Mater 7 (1995) 79–81.
[5] M. Zhou, C. Li, X. Li, J. Yao, Y. Wu, $K_2Sn_2ZnSe_6$, $Na_2Ge_2ZnSe_6$, and $Na_2In_2GeSe_6$: a new series of quaternary selenides with intriguing structural diversity and nonlinear optical properties, Dalton Trans. 45 (2016) 7627–7633.
[6] G. Li, K. Wu, Q. Liu, Z. Yang, S. Pan, $Na_2ZnGe_2S_6$: a new infrared nonlinear optical material with good balance between large second-harmonic generation response and high laser damage threshold, J. Am. Chem. Soc. 138 (2016) 7422–7428.
[7] G. Li, Q. Liu, K. Wu, Z.-H. Yang, S.-l. Pan, $Na_2CdGe_2Q_6$ (Q = S, Se): two metal-mixed chalcogenides with phase-matching abilities and large second-harmonic generation responses, Dalton Trans. 46 (2017) 2778–2784.
[8] H.W. Huang, J.Y. Yao, Z. Lin, X.Y. Wang, R. He, W.J. Yao, N.X. Zhai, C.T. Chen, Molecular engineering design to resolve the layering habit and polymorphism problems in deep UV NLO crystals: new structures in MM'$Be_2B_2O_6F$ (M = Na, M' = Ca; M = K, M' = Ca, Sr), Chem. Mater. 23 (2011) 5457.
[9] G.S. Yang, G. Peng, N. Ye, J.Y. Wang, M. Luo, T. Yan, Y.Q. Zhou, Structural modulation of anionic group architectures by cations to optimize SHG effects: a facile route to new NLO materials in the $ATCO_3F$ (A = K, Rb; T = Zn, Cd) series, Chem. Mater. 27 (2015) 7520.
[10] H. Huang, J. Yao, Z. Lin, X. Wang, R. He, W. Yao, N. Zhai, C. Chen, $NaSr_3Be_3B_3O_9F_4$: a promising deep-ultraviolet nonlinear optical material resulting from the co-operative alignment of the $[Be_3B_3O_{12}F](10-)$ anionic group, Angew. Chem. Int. Edit. 50 (2011) 10274.
[11] J. Pilmé, J.-P. Piquemal, Advancing beyond charge analysis using the electronic localization function: Chemically intuitive distribution of electrostatic moments, J. Comput. Chem. 29 (2008) 1440.
[12] D.E. Aspnes, Energy-band theory of the second-order nonlinear optical susceptibility of crystals of zinc-blende symmetry, Phys. Rev. B 6 (1972) 4648.
[13] J.E. Sipe, and E. Ghahramani, Nonlinear optical response of semiconductors in the independent-particle approximation, Phys. Rev. B 48 (1993) 11705.
[14] C. Aversa, J.E. Sipe, Nonlinear optical susceptibilities of semiconductors: results with a length-gauge analysis, Phys. Rev. B 52 (1995) 14636.
[15] S. Sharma, J.K. Dewhurst, C. Ambrosch-Draxl, Linear and second-order optical response of III-V monolayer superlattices, Phys. Rev. B 67 (2003) 165332.
[16] http://elk.sourceforge.net/.
[17] F. Tran, P. Blaha, Accurate band gaps of semiconductors and insulators with a semilocal exchange-correlation potential, Phys. Rev. Lett. 102 (2009) 226401.
[18] M.A.L. Marques, M.J.T. Oliveira, T. Burnus, Libxc: a library of exchange and correlation functionals for density functional theory, Comput. Phys. Commun. 183 (2012) 2272–2281.
[19] A.D. Becke, K.E. Edgecombe, A simple measure of electron localization in atomic and molecular systems, J. Chem. Phys. 92 (1990) 5397.
[20] R.F.W. Bader, Atoms in Molecules, a Quantum Theory, Oxford University Press, Oxford, 1990.
[21] G. Kresse, D. Joubert, From ultrasoft pseudopotentials to the projector augmented-wave method, Phys. Rev. B 59 (1999) 1758.
[22] H.J. Monkhorst, J.D. Pack, Special points for Brillouin-zone integrations, Phys. Rev. B 13 (1976) 5188.
[23] A. Savin, O. Jepsen, J. Flad, L.K. Anderson, H. Preuss, H.G. von Schnering, Electron localization in solid-state structures of the elements: the diamond structure, Angew. Chem. Int. Ed. Engl 32 (1992) 187.
[24] R.J. Gillespie, R.S. Nyholm, Inorganic stereochemistry, Quart. Rev. 11 (1957) 339.
[25] D. Kozlowski, J. Pilmé, New insights in quantum chemical topology studies using numerical grid-based analyses, J. Comput. Chem. 32 (2011) 3207.
[26] R.F.W. Bader, P.M. Beddall, P.E. Cade, Partitioning and characterization of molecular charge distributions, J. Am. Chem. Soc. 93 (13) (1971) 3095–3107.
[27] K.E. Laidig, R.F.W. Bader, Properties of atoms in molecules: atomic polarizabilities, J. Chem. Phys. 93 (1990) 7213.
[28] P.L.A. Popelier, Atoms in Molecules: an Introduction, Prentice-Hall, Harlow, U. K, 2000.
[29] B. de Courcy, L.G. Pedersen, O. Parisel, N. Gresh, B. Silvi, J. Pilmé, J.-P. Piquemal, Understanding selectivity of hard and soft metal cations within biological systems using the subvalence concept. I. Application to blood coagulation: direct cation-protein electronic effects vs. indirect interactions through water networks, J. Chem. Theory Comput. 6 (4) (2010) 1048–1063.
[30] F. Fedorov, Theory of Elastic Waves in Crystals, Plenum, New York, 1968, p. 33.
[31] M. Born, K. Huang, Dynamical Theory and Experiment vol. 1, Springer, Berlin, 1982.
[32] Z.J. Wu, E.J. Zhao, H.P. Xiang, X.F. Hao, X.J. Liu, J. Meng, Crystal structures and elastic properties of superhard IrN_2 and IrN_3 from first principles, Phys. Rev. B 76 (2007) 054115.
[33] G. Li, K. Wu, Q. Liu, Y. ZhiHua, S.-L. Pan, $Na_2ZnSn_2S_6$: a mixed-metal thiostannate with large second-harmonic generation response activated by penta-tetrahedral $[ZnSn_4S_{14}]^{10-}$ clusters, Sci. China Technol. Sci. 60 (2017) 1465.
[34] J.I. Jang, A.S. Haynes, F.O. Saouma, C.O. Otieno, M.G. Kanatzidis, Broadband studies of the strong mid-infrared nonlinear optical responses of $KPSe_6$, Opt. Mater. 3 (2013) 1302.
[35] J. Pilmé, E. Renault, A. Tahra, G. Montavon, N. Galland, Introducing the ELF topological analysis in the field of quasirelativistic quantum calculations, J. Chem. Theory Comput. 8 (2012) 2985.
[36] X. Krodikis, S. Noury, B. Silvi, Characterization of elementary chemical processes by catastrophe theory, J. Phys. Chem. 101 (1997) 7277.
[37] J.A. Brant, D.J. Clark, Y.S. Kim, J.I. Jang, J.-H. Zhang, J.A. Aitken, Li_2CdGeS_4, a diamond-like semiconductor with strong second-order optical nonlinearity in the infrared and exceptional laser damage threshold, Chem. Mater. 26 (2014) 3045–3048.
[38] K.P. Devlin, A.J. Glaid, J.A. Brant, J.-H. Zhang, M.N. Srnec, D.J. Clark, Y.S. Kim, J.I. Jang, K.R. Daley, M.A. Moreau, J.D. Madura, J.A. Aitken, Polymorphism and second harmonic generation in a novel diamond-like semiconductor: Li_2MnSnS_4, J. Solid State Chem. 231 (2015) 256–266.
[39] J.W. Lekse, B.M. Leverett, C.H. Lake, J.A. Aitken, Synthesis, physicochemical characterization and crystallographic twinning of Li_2ZnSnS_4, J. Solid State Chem. 181 (2008) 3217–3222.
[40] I. Merad-Boudia, A.H. Reshak, T. Ouahrani, Z. Bentalha, Density functional theory calculation of the optical properties and topological analysis of the electron density of $MBi_2B_2O_7$ (M = Ca, Zn) compounds, J. Appl. Phys. 113 (2013) 083505.
[41] D.A. Kleinman, Nonlinear dielectric polarization in optical media, Phys. Rev. 126 (1962) 1977–1979.